CONFERENCE PRE-PRINT

FIRST SOLPS-ITER WIDE GRID SIMULATIONS OF THE ITER BURNING PLASMA SCRAPE-OFF LAYER

E. KAVEEVA, N. SHTYRKHUNOV, V. ROZHANZKY, I. SENICHENKOV
Peter the Great St. Petersburg Polytechnic University
St. Petersburg, Russian Federation
Email: E.Kaveeva@spbstu.ru

R.A. PITTS, X. BONNIN, A. PSHENOV
ITER Organization
St Paul Lez Durance Cedex, France

Abstract

For the first time with the SOLPS-ITER code (using the recently code version 3.2.0), plasma boundary modelling with numerical grids extending to all main chamber surfaces under Q = 10 burning plasma conditions has been performed. This provides main wall fluxes of main ions and seeded (neon) impurities, key for more realistic estimates of wall power fluxes and providing a means to derive tungsten (W) influxes for assessments of impact on burning plasma performance in the recent ITER re-baseline with a full W main wall. Scans (without drifts and currents activated) have been performed over a range of radial transport coefficients in the far scrape-off layer. The choice of this range, and in particular the radial variation of the coefficients, is guided by estimates based on the assumption of cross-field filamentary (blobby) transport.

1. INTRODUCTION

One of the key problems of a tokamak fusion reactor is how the energy from the confined plasma will distribute over the different plasma-facing components (PFC). On the one hand, the heat loads on the divertor targets and other material surfaces should stay below engineering limits, while on the other, sputtering of PFCs should be low enough to have modest impact on the core plasma. These requirements are assumed to be satisfied by deuterium (D) gas puff and a simultaneous seeding of radiating species such as neon (Ne) or argon (Ar) to maintain the divertor in the semi-detached regime [1]. The choice of the reactor scenario is based heavily on the boundary plasma modeling performed with large simulations codes (e.g. SOLPS-ITER [2], SOLEDGE3X [3] etc.)

To date, the SOLPS code (and in particular the SOLPS-ITER versions [2]) has been the workhorse for the design and performance assessment of the ITER divertor (see [1] and references therein). Until very recently, the SOLPS simulation domain in most modelling studies has been restricted to an area outside the separatrix in the scrape-off layer (SOL) limited by a last flux surface which connects the two divertor targets of a single null configuration and just avoids intersecting any other surface of the main chamber walls. It therefore plays the role of an artificial first wall (FW). The boundary conditions for the plasma equations are imposed on this last flux surface so that recycling, sputtering and heat loads associated with plasma can be calculated there. The region between the last flux surface and the real PFCs contains only neutral particles, and no ionization is assumed there. Meanwhile, plasma parameters in this area are approximated using decay profiles from the simulation region. Such an approach leads to large uncertainties in the far-SOL plasma parameters and therefore to uncertainties in the predictions of PFC heat loads and sputtering. This latter quantity has taken on far greater significance as a result of the recent ITER re-baselining in which the beryllium main chamber armour in the 2016 Baseline has been replaced by tungsten (W) [4]. Given the strong impact of high Z species on fusion plasma performance and the poor screening of the main SOL plasma (compared with the divertor) for impurities released from FW surfaces, more accurate assessments of the ITER W wall source are crucial.

To overcome this deficiency in the ability of SOLPS to solve out to all wall surfaces, in the last few years a wide unstructured grid approach has been developed [5], so that plasma simulations can be performed up to the real surfaces with the boundary conditions imposed on the real constructions. This “wide grid” capability has actually been the default in the more modern code SOLEDGE3X [3] which has now been applied to ITER simulations for both low power initial operation [6] and even for some preliminary studies in Ne-seeded burning plasmas [7]. A benchmarking effort is now possible, and is underway, between the two codes (SOLPS-ITER and SOLEDGE3X) on wide grids.

When modelling on wide grids, several issues need to be addressed. The first is connected with the applicability of the fluid equations in the far SOL. Since the electron density in this region is rather low, plasma is usually in the sheath-limited regime with large collisional mean-free-paths. As a consequence, correct flux-limiting coefficients should be used in the fluid Braginsky-type equations solved in fluid transport codes.

A second problem is the choice of transport coefficients both in the near and far SOL plasmas. As a near-SOL in this paper stands the region of few energy radial characteristic lengths, where typically the plasma solution is different from that further from separatrix, in the region called here far SOL. There is now a great deal of experimental evidence that transport in the far-SOL is different from that in the near SOL, often resulting in the formation of "shoulders" in the far SOL density profiles (see e.g. [8]-[9]) at the distance more than one or two centimeters from separatrix at the OMP. According to present day understanding, cross-field transport in a large fraction of the SOL radial range is controlled by radial propagation of field aligned filamentary structures sometimes referred to as blobs as a result of their appearance when viewed in the radial-poloidal plane (see [10] and references wherein). The filament velocity depends on plasma parameters (e.g. collisionality), but analytical estimates of effective turbulent transport are still missing, making the choice of SOL transport coefficients in the transport codes very difficult.

The third problem is connected with the wide range of magnetic field lines angles of intersection with the PFC in the far SOL. In many locations this can be such that the turbulent radial and parallel transport toward the wall being are of the same order. This in turn leads to numerical instabilities due to the abrupt change of the effective transport coefficients in the direction towards the wall. In addition, numerical issues caused by the sheath boundary conditions imposed on more than two cell faces bounding a flux tube of the calculation mesh need to be resolved.

In this paper we present estimates for anomalous transport coefficients based on physical analysis of filamentary transport which are consistent with experimental observations on present devices. These coefficients are then used in SOLPS-ITER simulations with unstructured wide grid (version 3.2.0 on extended grid) and with $\vec{E}\times\vec{B}$ drift and ∇B-drift switched off for simulations of the ITER baseline (burning plasma) scenario.

2. ESTIMATES FOR FAR SOL TRANSPORT COEFFICIENTS

2.1. Sheath limited regime

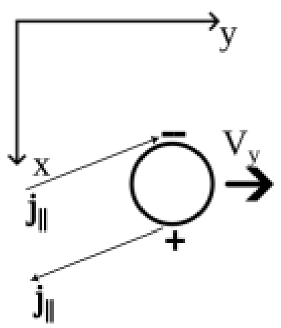

FIG.1. Polarization and parallel currents in the poloidal-radial plane in a filament.

The diffusion coefficient can be estimated for SOL plasma transport with the sequence of individual filaments. Three assumptions based on both modeling and experimental observations [10] need to be made:

1) Filaments in a range of some typical most stable dimensions follow each after the other, without big time delay.

2) The velocity of filaments can be estimated assuming that they are still electrically connected to the divertor targets. This assumption is based on the observation that in low collisionality case the filaments of a size corresponding to beginning of their electric disconnection from the target (at the boundary of sheath-connected regime and connected ideal-interchange regime [10]) are mainly observed in the modeling and experiment.

3) The typical filament radial propagation length is of the same order as its initial size. This assumption is based both on the modeling and analytical estimates, describing the decay of individual filaments.

A single filament with density δn is getting polarized by vertical ∇B- driven current $I_g=\frac{2\delta n(T_e+T_i)}{BR}l_{||}$ as shown in Fig.1. It is closed by the parallel current $j_{||}=I_g/l_\perp=\frac{2\delta n(T_e+T_i)l_{||}}{BRl_\perp}$, where $l_\perp$ is filament size in x-direction. Parallel current is connected with the potential perturbation according to the current-voltage characteristic of the sheath $j_{||}=enc_s\frac{e\delta\varphi}{T_e}$, so that the electrostatic potential perturbation is $\delta\varphi=\frac{2\delta n(T_e+T_i)T_e l_{||}}{nc_s e^2BRl_\perp}$. Radial filament velocity is determined by $\vec{E}\times\vec{B}$ drift: $V_y=\frac{2\delta n(T_e+T_i)T_e l_{||}}{nc_s e^2B^2Rl_\perp^2}$.

The estimate can be made for the density perturbation in the filament propagating radially on the distance $l_\perp$ of the same order as its poloidal dimension: $\delta n=l_\perp\frac{\partial n}{\partial \mathrm{r}}=l_\perp\frac{n}{\lambda_n}$. Then the average radial flow associated with filaments following each after the other doesn't depend on their typical size $\langle\delta nV_y\rangle=\frac{2n(T_e+T_i)T_e l_{||}}{c_s e^2B^2R\lambda_n^2}$.

The corresponding estimate for the SOL radial scale for density then follows from the balancing of radial flow divergence and the parallel flow divergence $\langle\delta nV_y\rangle/\lambda_n\approx nc_s/l_{||}$. This estimate is $\lambda_n\approx\left(\frac{2(T_e+T_i)T_e l_{||}^2}{e^2B^2Rc_s^2}\right)^{1/3}$.

The estimate for diffusion coefficient can be done $D \approx \left(\frac{2(T_e+T_i)T_e}{e^2B^2}\right)^{2/3}\left(\frac{q}{c_sR}\right)^{1/3}$ from the balancing of radial diffusive flow divergence and the parallel flow divergence $Dn/\lambda_n^2 \approx nc_s/l_{||}$.

2.2. Conduction limited regime

The strike-point and near-SOL detachment is mandatory for target protection in full burning ITER scenario leading to the choice of semi-detachment as a main working divertor regime. Semi-detachment can be attained in vertical divertor targets configuration in which due to reflection of neutral particles towards the private flux region the neutrals density is elevated in the strike point vicinity and is strongly decreased in the far SOL comparing to configuration of divertor with horizontal targets. Therefore, the flux tubes closest to the strike point detach first when impurity seeding or neutrals pressure in the divertor are increased. The zones along the divertor target are situated then as follows: strike-point and at least near SOL (2-3 energy radial characteristic lengths) detached – necessary for target protection; some part of SOL further from strike point – conduction limited; even further – sheath limited [11]. The comparative dimensions of these zones are controlled by divertor neutral pressure and by impurity seeding, which can vary considerably still keeping divertor in acceptable working semi-detached regime. Full detachment of divertor is now not discussed as standard regime for ITER since in nowadays tokamaks it is typically accompanied by X-point radiator, which demands special control. So, in the present work modifications of the estimates given in Section 2.1 for conduction-limited or detached parts of divertor target are appropriate. The plasma density at these parts of the target is generally much higher than that in the equatorial midplane. As a consequence, the parallel current, which is proportional to the filament density δn, is more easily closed so that the polarization potential is reduced, the filament velocity decreases, and the turbulent diffusion coefficient due to this effect can be lower than in the far-SOL. Formally one has to substitute target parameters into the sheath current-voltage characteristic, while keeping upstream parameters in the ∇B-current (I_g) and in the particle balance.

Counteracting this reduction in radial velocity, due to finite conductivity a significant potential drop along the flux tube on which the filament resides may be required to drive the closing parallel current. This effect leads to an increase in the filament radial velocity. To quantify these effects the sheath effective resistivity parameter can be introduced $R_{sh} = \frac{\varphi_{sh}}{j_{||OMP}} = \frac{B_t}{B_{OMP}}\frac{T_{et}}{e^2 n_t c_{s_t}}$, where the ratio $\frac{B_t}{B_{OMP}}$ represents a flux expansion from OMP to target, which will always be present in tokamak geometry (subscripts *t* and *OMP* respectively refer to values at the divertor target and the outer midplane taken as representative of "upstream"). An effective volume resistivity parameter is also introduced as $R_{vol} = \frac{\varphi_{OMP}-\varphi_{sh}}{j_{||OMP}} = \frac{1}{B_{OMP}}\int_{OMP}^{t}\frac{Bh_x dx}{\sigma_{||}b_x}$, where h_x is the Lamé coefficient for the real geometry. Combining both resistivity parameters, the flux tube current-voltage characteristic reads $j_{\|_{OMP}} = \frac{\varphi_{OMP}-\varphi_{plate}}{R_{sh}+R_{vol}}$, and the filament velocity should be multiplied by a factor $\frac{R_{vol}+R_{sh}}{R_{shOMP}}$, where $R_{sh_{OMP}} = \frac{T_{OMP}}{e^2 n_{OMP} c_{s_{OMP}}}$. Finally the estimate for the diffusion coefficient can be obtained:

$$D = \left(\frac{T_{eOMP}}{e}\right)^{4/3} B^{-4/3}\left(1+\frac{T_{iOMP}}{T_{eOMP}}\right)^{2/3}\left(\frac{4r}{R^2 b_x c_s}\right)^{1/3}\left(\frac{R_{vol}+R_{sh}}{R_{shOMP}}\right)^{2/3} \quad (1)$$

This estimate is also valid in the case when the filament is disconnected from the target and the ∇B-current is compensated by polarization current in the divertor, if the plasma resistivity between the divertor and upstream plays the major role in the filament potential formation (so called resistive X-point regime of Refs. [10]).

3. MODELING RESULTS

3.1 Choice of transport coefficients

The values R_{sh} and R_{vol} were obtained from SOLPS-ITER simulations for the baseline ITER scenario with Ne seeding [12] and for ASDEX-Upgrade H-mode scenarios [13] with different levels of impurity seeding and, as a consequence, different degrees of divertor partial detachment. Compared to the sheath-limited regime, the decrease of R_{sh} and the increase of R_{vol} at the parts of divertor target that are in conduction limited regime roughly compensate each other. Thus, the estimate for the total resistivity parameter based on the upstream parameters and the sheath limited approximation remains valid in semi-detached regime. For the ASDEX-Upgrade pronounced detachment regime, T_{et} ~ 6 eV everywhere along the target, the sum of sheath and volume resistivity parameters in the near SOL increases by a factor of 10 compared to that for the attached regime, and the diffusion coefficient is expected to increase.

For the semi-detached ASDEX-Upgrade case with 50% of radiation, the diffusion coefficient may be estimated from Eq.(1) taking the SOL parameters at the OMP. Choosing $\frac{T_e}{e} = 20\ eV, B = 2T, \frac{T_i}{T_e} = 2,\ b_x = 0.1, R = 1.75\ m, r = 0.5\ m$ the diffusion coefficient $D = 2.2 m^2/s$ is obtained. The corresponding density decay length is $\lambda_n = 1.4\ cm$. According to the authors' experience from fitting experimental ASDEX Upgrade SOL profiles during the SOLPS-ITER modelling exercise, this estimated effective diffusion coefficient is in reasonable agreement with the values typically required in this modelling (D = 1.5 m^2/s [14]). For ITER H-modes, the SOL T_e and toroidal magnetic field will be around a factor of 2 higher than in ASDEX-Upgrade. According to Eq.(1), this would yield a diffusivity of $D = 2.0 m^2/s$ and therefore very similar to that in ASDEX-Upgrade in the region with dominating filamentary transport mechanism.

Following these arguments, for the ITER modeling described below we may set the far SOL anomalous diffusivity to $D_{AN,farSOL} = 2\ m^2/s$. The diffusivity coefficient may then be varied around this value to see the effect of this variation on the fluxes to the FW, Fig.1. It is important to note, however, that in the majority of ITER modeling studies performed to-date with the SOLPS code suite on standard structured grids (including those conducted by the present authors), $D_{AN,farSOL}$ was set to $0.3\ m^2/s$ so it is important for benchmarking purposes to preserve this setting for some of the new runs on the unstructured (wide grid) SOLPS-ITER 3.2.0. Further increases of $D_{AN,farSOL}$ up to $5\ m^2/s$ or $10\ m^2/s$ are also considered to explore the impact of forcing extremely broad shoulders on the far-SOL fluxes.

The near-SOL width where the transport coefficients in Fig.1 stay unmodified as they were chosen in previous modeling studies, denoted here by parameter L, was chosen equal to 1 or 3 cm. The smaller value, $L = 1\ cm$ is higher than the value of the near-SOL power width, $\lambda_{q,nearSOL} \approx 3.5\ mm$ (see Fig. 4 of [1]), typically associated with previous SOLPS modelling of ITER burning plasmas, but is lower than the characteristic length ($\lambda_{n,nearSOL}$~3 cm) of the density profile in the structured grid modeling set-up [1]. Such a choice is expected to provide conservation of $\lambda_{q,nearSOL}$ making at the same time significant effect on the density distribution. The higher value $L = 3\ cm$ is chosen to be comparable to $\lambda_{n,nearSOL}$. Such choice should lead to more moderate effect on the density profile, since at the boundary of region where the transport is decreased the density is already significantly lower than at separatrix. The transition from near to far SOL for ITER can be defined only in the turbulent modeling. Still, the chosen values should cover the wide range of possibilities.

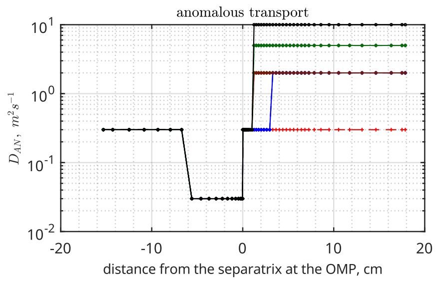

FIG. 2. Diffusion coefficients at the OMP. The points on each line represent the radial locations of the mesh points and thus illustrate the grid resolution.

For each case the turbulent heat conductivities $\chi_{i,AN}$, $\chi_{e,AN}$ and viscosity ν_{AN} are increased by the same factor as for $D_{AN,farSOL}$, both in the main SOL and in the corresponding flux tubes in the divertor region. An anomalous pinch velocity is not imposed, $V_{AN} = 0\ m/s$.

3.2 Benchmarking with standard structured grid SOLPS-ITER modeling

For the wide-grid versus standard structured grid benchmarking, the lowest ($D_{AN,farSOL} = 0.3\ m^2/s$) anomalous transport coefficients are used (red dashed line in Fig. 2). Deuterium gas puffing is set to $5 \cdot 10^{22} s^{-1}$, and the neon seeding is varied from $6.75 - 12 \cdot 10^{19} s^{-1}$ for the standard grid and from $4.5 - 9 \cdot 10^{19} s^{-1}$ for the wide grid case. The pumping coefficient is set by a feedback scheme to achieve a D atom and molecule pressure in the private flux region (PFR) of $p_D = 7\ Pa$. The particle fluxes from the core region are: $\Gamma_D = 1 \cdot 10^{22} s^{-1}$, $\Gamma_{He} = 1 \cdot 10^{20} s^{-1}$ and the input power equally shared between electrons and ions is $P_{e+i} = 100\ MW$. The computational meshes are shown in Fig. 3a, where the wall contour is used from shot IMAS #116000, run#4. This magnetic equilibrium and wall contour, which is the most up-to-date description for burning plasma studies, has a distance between primary and secondary separatrices at the OMP of ~6.5 cm, $B_t = 5.3\ T$, $I_p = 15\ MA$. In the modelling, the current continuity equation is solved, but the drift terms both in the electric current and ion transport are not taken into account. Nevertheless, the solution of this equation gives the thermoelectric current distribution, which influence the particle and heat flows to the material surfaces.

Both the OMP and target profiles (not shown here) are similar for the standard and wide-grid meshes in the near SOL. The latter are the same near the strike-points, but differences appear at distances of ~5 cm from strike-point, leading to moderate difference in the target heat load. Fig. 3(b) gives the dependency of peak outer target heat load on neon concentration at the separatrix and on p_D. There is only a relatively small discrepancy in the narrow and wide grid modeling results for this parameter. From this first, somewhat restricted benchmarking exercise, it can be concluded that in the near-SOL the calculations on standard and wide meshes give approximately similar results.

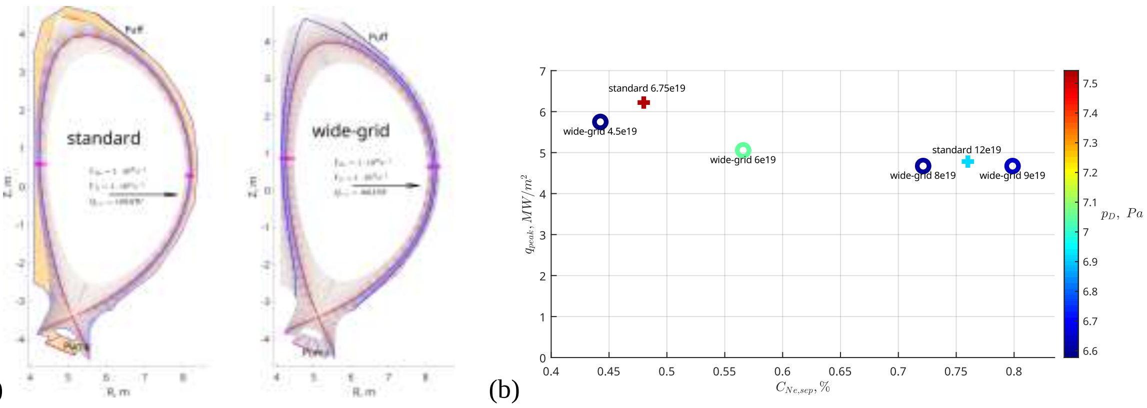

(a) (b)

FIG.3: (a) Computational domain for standard and wide-grid simulations. The B2.5 and EIRENE computational meshes are shown in purple and orange respectively. Primary and secondary separatrices respectively in red and blue, the cells centers chosen to plot inner and outer midplane parameters are marked by the pink circles. The fuel gas puffing and Ne seeding areas are given by the dark blue line and the pumping surface by the dark purple line. The green lines in the PFR denote surfaces at which P_D is calculated. (b) Peak outer target strike point heat flux density versus Ne concentration (computed as the ratio to electron density). Pressure of neutral D is shown via the colorbar. The Ne seeding values are used as labels of the runs.

3.3. Transport coefficient scan in wide grid modeling

Here we focus on the results of scanning the cross-field transport coefficients and their radial profiles (see Fig. 2) for the wide-grid mesh (Fig. 3a, right). Ne seeding is set by a feedback scheme to achieve prescribed values of $C_{Ne} = 0.4\%$ or $C_{Ne} = 1.2\%$. All other modelling set-up parameters are as used in the wide-grid benchmarking study of the previous section.

Plasma profiles at the OMP are shown in Fig.4, with the dashed and solid lines corresponding to the cases with $C_{Ne} = 0.4\%$ and $C_{Ne} = 1.2\%$ respectively. Table 2 collects the characteristic decay lengths λ_{T_i}, λ_{T_e} and λ_n of T_e, T_i and n_e respectively in far SOL. They are evaluated by exponential fitting of radial profiles in the far-SOL at a distance > 10 cm from the separatrix at the OMP (Fig. 4). Fig.5 gives the radial fluxes of the main ions and heat integrated along the closed flux surfaces in the confined region and along flux surfaces from X-point to X-point in the SOL. For cases with $D_{AN,farSOL} \geq 5\, m^2/s$ the ion flow through the separatrix is considerably higher than in the other cases. This is a consequence of a higher ionization source inside the separatrix. For the very high transport coefficients the main chamber wall recycling is more intense, leading to a higher neutral influx from the wall. At the same time, the electron density near the separatrix is lower when radial transport is higher making the SOL more transparent to neutrals. As a result, n_e, T_i and T_e inside the separatrix start to change significantly compared to the cases with lower far-SOL transport. Electron density rises from approximately $1 \cdot 10^{20} m^{-3}$ up to $1.75 \cdot 10^{20} m^{-3}$. Ion and electron temperatures drop from $3100\ eV$ to $1300\ eV$, mainly because the radial heat conductivity is proportional to the density.

Figs. 6 and 7 compile profiles of n_e, T_e, T_i, D and Ne ion fluxes and average charge of Ne along the FW and the divertor targets with reference point at the OMP. There is a noticeable rise of temperatures at the IMP: T_e and T_i increase from 3 - 18 eV and 7 - 85 eV respectively. At the top of the main chamber a temperature decrease and electron density peak are observed, corresponding to the secondary X-point position. This may also be seen clearly in the 2D T_i profiles of Fig. 6. At the targets the temperatures are low near the strike points (~1 eV) for all cases, and increase in the far-SOL with increasing radial transport (peak far-SOL T_e and T_i range from 13 - 26 eV and 40 - 90 eV respectively.

TABLE 1: EXPONENTIAL DECAY LENGTHS OF MAIN PLASMA PARAMETERS

Label	C_{Ne}, %	λ_{T_e}, cm	λ_{T_i}, cm	λ_n, cm
D=0.3	0.4	3.7	7.8	1.7
D=2,L=3	0.4	5.3	13.1	2.9
D=2,L=1	0.4	5	12.5	2.7
D=5,L=1	0.4	5.8	22.5	3.6
D=2,L=3	1.2	5.2	12.9	2.9
D=2,L=1	1.2	5	12.2	2.7
D=5,L=1	1.2	6.1	20.4	3.6
D=10,L=1	1.2	6.8	35.3	4.8

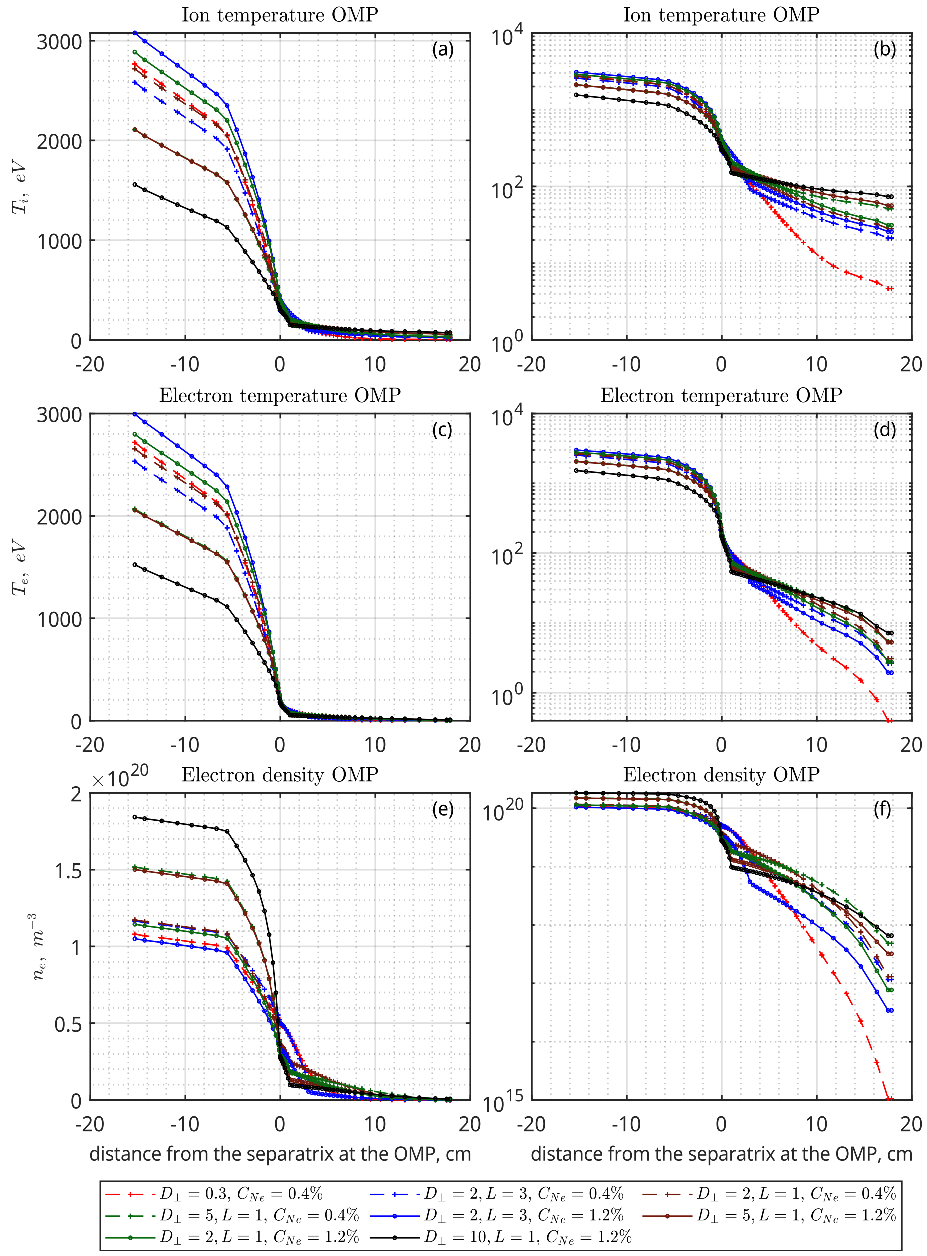

FIG. 4. Profiles of T_e (a,b), T_i (c,d) and n_e (e,f) at the OMP (linear and logarithmic scales) for varying strength and radial profile of anomalous transport

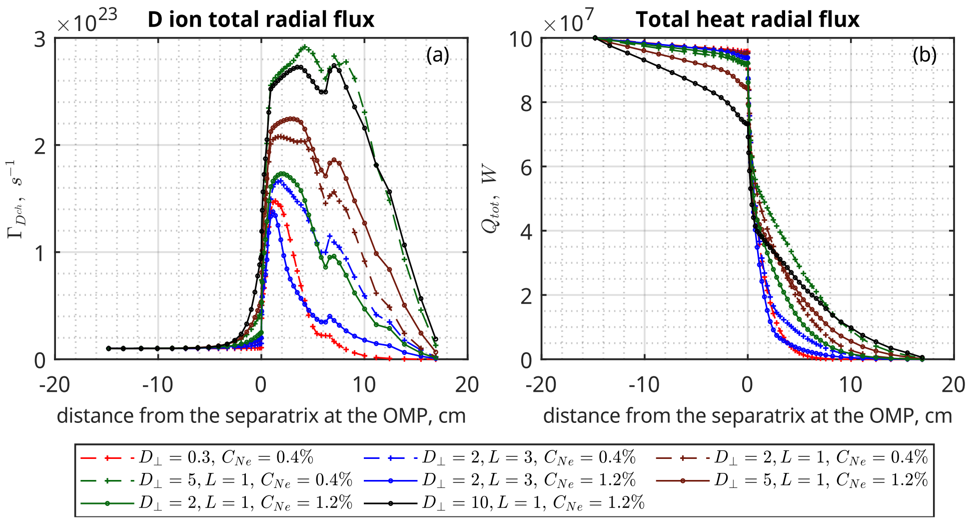

FIG. 5. Total radial deuterium ion flux (a) and total radial heat flux (b)

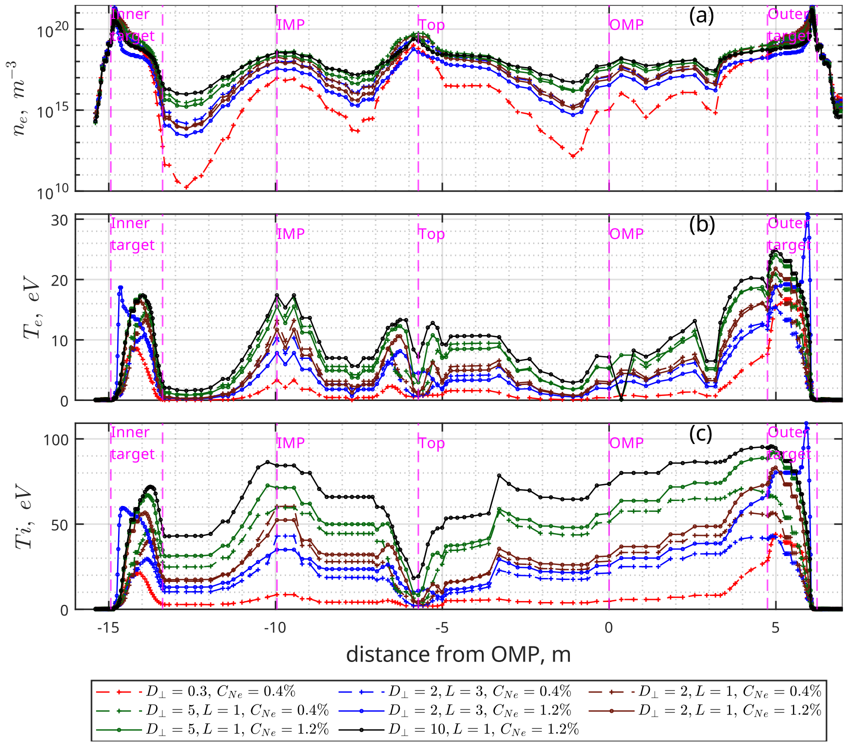

FIG. 6. Profiles of n_e (a), T_e (b), T_i (c) along the wall. IMP denotes inner midplane.

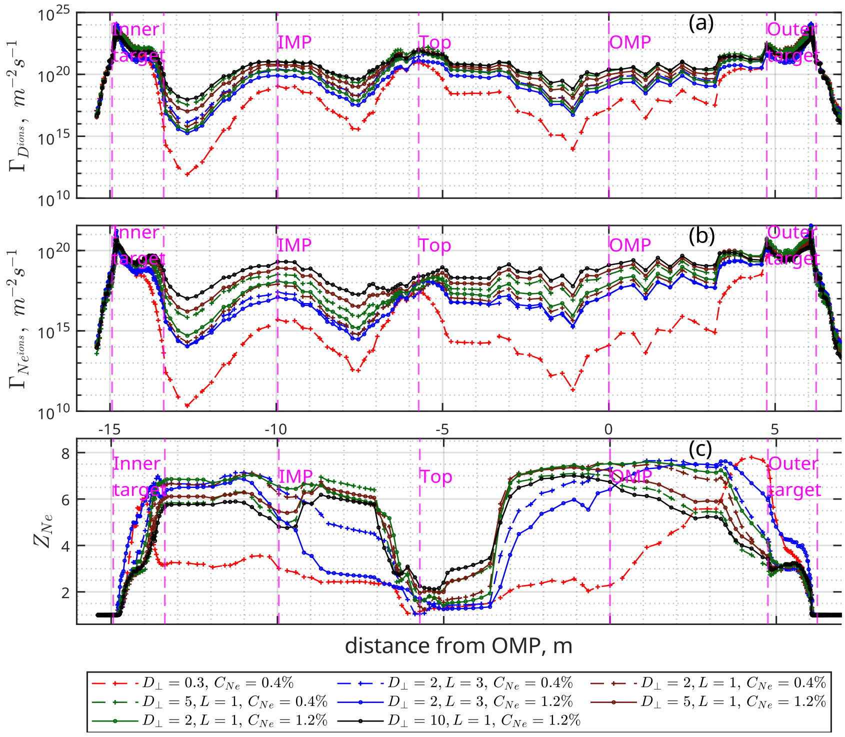

FIG.7. Profiles of D ion flux (a), Ne ion flux (b) and average charge on Ne (c) along the wall. IMP denotes inner midplane.

4. DISCUSSION AND CONCLUSIONS

The first modeling of ITER burning plasmas, including impurity (Ne) seeding for divertor power flux control, with the new SOLPS-ITER 3.2.0 code version featuring a wide-grid capability allowing the computational mesh to be extended to the main chamber walls has been performed. The primary objectives of these numerical studies are a more realistic description of the plasma flows onto the wall, and the production of simulated plasma backgrounds which can later be used by other codes for the study of tungsten sputtering and migration. For the first time for such a scenario convergence of SOLPS-ITER 3.2.0 was achieved with the equation for the electrostatic potential included in the calculations.

The SOLPS-ITER 3.2.0 results were compared with those from SOLPS-ITER 3.0.8 simulations performed on the standard narrower grid which has hitherto dominated all SOLPS studies for ITER. The comparison was performed for constant moderate SOL transport level, previously typically used for ITER modeling. In the common computational domain both the wide and narrow grid codes yield closely similar results.

In a subsequent study, focusing only on the wide-grid simulations, the cross-field transport coefficients in the far-SOL were increased in order to simulate the possible widening of SOL (the so-called shoulder formation) due to increased convective (filamentary) transport. The typical effective diffusivity values in the SOL region of filamenary transport, used in the modeling, are based on the simple but robust model estimates, presented in the paper. The transport parameters were varied over a wide range around the values expected from estimates as well as the distance from separatrix where the filamentary transport starts to dominate and the transport needs to be increased. As a result, in the limiting case of factor 30 the characteristic density scale length in the far-SOL has increased approximately by factor of 3. The electron temperature decreases at scales comparable to those of density, while the ion temperature decreases considerably more slowly. The ion temperature decay length can exceed 10 cm, leading to high (of the order of several tens of eV) ion temperature at the wall.

An increase of the diffusion coefficient up to values $D_{AN,farSOL} \geq 5\, m^2/s$ leads to an increase of the ionization source inside the separatrix. For lower values of the diffusion coefficient, obtained from estimates based on simple models of filamentary transport and for modeling of semi-detached regimes of modern tokamaks, the far-SOL transport does not significantly affect the plasma parameters inside the separatrix. At the same time the flow of main ions and seeded impurity to the wall at the outer and inner midplanes increases by approximately two orders of magnitude when the diffusion coefficient increases from $D_{AN,farSOL} = 0.3\, m^2/s$ to $D_{AN,farSOL} = 2\, m^2/s$. The latter value can be taken as a reasonably pessimistic scenario.

ACKNOWLEDGEMENTS

This work was supported by the ITER International Fusion Energy Organization Service Contract No. IO/23/CT/4300002968 of 24.11.2023. This work was performed under the auspices of the ITER Scientist Fellow Network. The views and opinions expressed herein do not necessarily reflect those of the ITER Organization. Numerical calculations were performed at the Polytechnic Supercomputer Center at Peter the Great St. Petersburg Polytechnic University

REFERENCES

[1] PITTS, R. A. et al, Physics basis for the first ITER tungsten divertor, Nucl. Mater. Energy **20 (**2019) 100696
[2] BONNIN, X. et al., Presentation of the new SOLPS-ITER code package for tokamak plasma edge modelling, Plasma Fusion Res. **11** (2016) 1403102
[3] BUFFERAND, H. et al., Progress in edge plasma turbulence modelling—hierarchy of models from 2D transport application to 3D fluid simulations in realistic tokamak geometry, Nucl. Fusion **61** (2021) 116052
[4] PITTS, R. A. et al., Plasma-wall interaction impact of the ITER re-baseline, Nucl. Mater. Energy **42** (2025)101854
[5] DEKEYSER, W. et al., Plasma edge simulations including realistic wall geometry with SOLPS-ITER, Nucl. Mater. Energy **27 (**2021**)** 100999
[6] RIVALS, N. et al., SOLEDGE3X full vessel plasma boundary simulations of ITER non-active phase plasmas, Nucl. Fusion **65 (**2025**)** 026038
[7] SURESHKUMAR, S. et al., First SOLEDGE3X-EIRENE simulations of the ITER Neon seeded burning plasma boundary up to the first wall, Nucl. Mater. Energy **41** (2024) 101780
[8] CARRALELO, D. et al., A study on the density shoulder formation in the SOL of H-mode plasmas, Nucl. Mater. Energy **12** (2017)1189
[9] EICH, T. et al., Turbulence driven widening of the near-SOL power width in ASDEX Upgrade H-Mode discharges, Nucl. Fusion **60** (2020) 056016
[10] D'IPPOLITO, D.A., MYRA, J.R., ZWEBEN, S.J. Convective transport by intermittent blob-filaments: Comparison of theory and experiment, Phys. Plasmas **18** (2011) 060501;
[11] KALLENBACH, A. et al., Partial detachment of high power discharges in ASDEX Upgrade, Nucl. Fusion **55** (2015) 053026
[12] ROZHANSKY, V. et al., Multi-machine SOLPS-ITER comparison of impurity seeded H-mode radiative divertor regimes with metal walls, Nucl. Fusion **61 (**2021**)** 126073
[13] SENICHENKOV, I. et al., Comparison of divertor seed impurity gases retention efficiency by SOLPS-ITER modeling, Nucl. Fusion **65** (2025) 056042
[14] ROZHANSKY, V., et al., Current structure in the scrape-off layer of a tokamak in a quiescent statePlasma Phys. Control. Fusion **63 (**2021**)** 015012